Author/s:
Zheng, F;Chen, W;Bu, T;Ghiggino, KP;Huang, F;Cheng, Y;Tapping, P;Kee, TW;Jia, B;Wen, X

Title:
Triggering the Passivation Effect of Potassium Doping in Mixed-Cation Mixed-Halide Perovskite by Light Illumination

Date:
2019-06-01

Citation:
Zheng, F., Chen, W., Bu, T., Ghiggino, K. P., Huang, F., Cheng, Y., Tapping, P., Kee, T. W., Jia, B. & Wen, X. (2019). Triggering the Passivation Effect of Potassium Doping in Mixed-Cation Mixed-Halide Perovskite by Light Illumination. Advanced Energy Materials, 9 (24), https://doi.org/10.1002/aenm.201901016.

Persistent Link:
https://hdl.handle.net/11343/285721

DOI: 10.1002/ ((please add manuscript number))

Article type: Full Paper

Triggering the Passivation Effect of Potassium Doping in Mixed-Cation Mixed-Halide Perovskite by Light Illumination

Fei Zheng,[+] Weijian Chen,[+] Tongle Bu, Kenneth P. Ghiggino, Fuzhi Huang, Yibing Cheng, Patrick Tapping, Tak W. Kee, Baohua Jia, Xiaoming Wen**

[+] These authors contributed equally to this work

Dr. F. Zheng,[+] Dr. W. Chen,[+] Prof. B. Jia*, Dr. X. Wen,*

Centre for Translational Atomaterials,

Swinburne University of Technology,

Hawthorn Victoria 3122, Australia
E-mail: bjia@swin.edu.au, xwen@swin.edu.au

T. Bu, Prof. F. Huang, Prof. Y. Cheng

State Key Laboratory of Advanced Technology for Materials Synthesis and Processing,

Wuhan University of Technology,

Wuhan, Hubei Province, 430070, P. R. China

Dr. F. Zheng,[+] Prof. K. P. Ghiggino

ARC Centre of Excellence in Exciton Science, School of Chemistry, The University of Melbourne, Parkville, Victoria 3010, Australia

Dr. P. Tapping, A.Prof. T. W. Kee

Department of Chemistry,

The University of Adelaide,

Adelaide, South Australia 5005, Australia

Keywords: Perovskite; Potassium (K^+) doping; Passivation; Light Soaking; Photoluminescence

Abstract:

Potassium (K^+) doping has been recently discovered as an effective route to suppress hysteresis and improve the performance stability of perovskite solar cells (PSCs). However, the mechanism of these K^+ doping effects is still under debate, and rationalization of the improved performance in these perovskites is needed. Herein, we dynamically monitor the PL properties and device performance of mixed-cation mixed-halide perovskite with and without K^+ doping under bias light illumination via a confocal fluorescence microscope, together with ultrafast transient absorption as well as time-dependent and time-resolved PL measurements. We demonstrated that illumination is essential to trigger the passivation effect of K^+ by forming KBr-like compounds, leading to the elimination of interface trapping defects and suppression of mobile ion migration, thus resulting in improved power conversion efficiency and negligible current-voltage hysteresis of solar cells. This work provides novel insight into the hysteresis suppression upon K^+ doping and highlights the significance of light illumination when using this protocol.

1. Introduction

Organic-inorganic hybrid perovskite has attracted growing attention due to their great potential in low cost and flexible solar energy conversion applications.[1–4] The power conversion efficiency (PCE)

of perovskite solar cells (PSCs) have rapidly progressed from 3.8% to exceed 24.2% during the past decade.[5,6] To improve the thermal stability and broaden the absorption spectrum range of PSCs, mixed-cation mixed-halide perovskite ($FA_xMA_{1-x}PbI_yBr_{3-y}$) with band-gap tunability are widely used.[7,8] The recent trend of cation doping has seen the increase of A-site diversity away from purely organic cations such as methylammonium (MA^+) and formamidinium (FA^+), to complex cations composed of major organic cations doped with alkali cations such as cesium (Cs^+), rubidium (Rb^+), and potassium (K^+).[9–11] Triple- or quadruple-cation perovskites with a few percent of Cs^+, Rb^+ or K^+-doping have already been successfully achieved, demonstrating improved performance stability and suppressed J-V hysteresis in PSC devices.[12,13] Cs^+ doping into FA/MA-based perovskites can improve the structural stability by suppressing the formation of the orthorhombic δ-phase (non-photoactive "yellow phase"), achieving high-efficiency PSCs with stabilized PCE of 21.1%.[9] Further doping of triple cation CsFAMA perovskite by oxidation-stable rubidium cation (Rb^+) leads to low-voltage-loss PSCs with efficiencies of up to 21.6% and long-term device stability at elevated temperature.[10] More recently, the smaller alkali cation K^+ was introduced into CsFAMA perovskite to tune the film morphology and optoelectronic property.[13,14] The incorporation of K^+ effectively increases the grain size and reduces the interfacial defect density in the perovskite layer, leading to hysteresis-free, stable and high PCE (20.56%) quadruple-cation PSCs.[13]

Although great improvements in photovoltaic performance have been achieved by alkali cation doping, the precise role of these dopants in enhancing device stability is still unclear. According to Goldsmith's theory, only Cs^+ can form stable perovskite structures when occupying the A-site of the crystal lattice, with a tolerance factor ($t = (R_A + R_X)/\sqrt{2}\,(R_B + R_X)$, where R is the ionic radius) falling in the eligible range between 0.8 and 1.[15] Other alkali cations (Rb^+, K^+) are too small for

appropriate replacement of organic cations in the A-site and are believed to be located in the interstitial sites of the perovskite lattice.[16–18] Perovskite lattice expansion and corresponding bandgap variation upon incorporation of small radius alkali cations (Rb^+, K^+ and Na^+), were observed by X-ray diffraction and energy-dispersive X-ray spectroscopy.[11] Theoretical work based on density functional theory (DFT) calculations by Jie et al. unambiguously revealed size-dependent interstitial occupancy of these extrinsic alkali cations doped into CsFAMA perovskite,[19] where alkali cations in the interstitial sites of perovskite lattice suppresses the migration of halide ion defects by raising the energy barriers, resulting in reduced J-V hysteresis and improved photo-stability of PSCs upon K^+ doping. Meanwhile, Abdi-Jalebi et al. demonstrated that K^+ doping in mixed perovskites reduces non-radiative losses and photo-induced ion migration in perovskite films by decorating the surfaces and grain boundaries with passivating potassium halide layers.[20] In this point of view, potassium cations are mainly distributed at the surfaces and grain boundaries by forming KI/KBr to immobilize the surplus mobile halide ions and vacancies,[21] which is contradictory to the interstitial occupancy of K^+ in the perovskite lattice.[19,22] More recently, Dominik et al. provided atomic-level characterization of the K^+ doped perovskite, finding no evidence of K^+ incorporation into 3D perovskite lattices, but observed the formation of a mixture of potassium-rich phases instead.[23] The interplay between doped K^+ and mixed-cation mixed-halide perovskite is therefore still a topic of debate. Better understanding the doping mechanism of K^+ into mixed perovskites is urgently required to further optimize the potassium doping strategies in mixed-cation mixed-halide perovskite for long-term stable and hysteresis-free PSCs.

Our previous work demonstrated that 3.5 mol% molar ratio K^+ doping to mixed-cation lead mixed-halide $Cs_{0.05}(FA_{0.85}MA_{0.15})_{0.95}Pb(I_{0.85}Br_{0.15})_3$ (CsFAMA) perovskite is optimal to achieve a hysteresis-

free, high PCE PSC.[13] Herein, we further explored the mechanism of ion migration suppression in this perovskite film upon K^+ doping, combining ultrafast, time-resolved and micro-spectroscopic techniques. By simultaneously mapping the PL intensity and lifetime of the perovskite during light soaking, dynamic fluorescence lifetime imaging microscopy (FLIM) revealed a consolidated and homogeneous photophysical property change in the K^+ doped perovskite. A gradual halide ion substitution of Br^- by I^- occurred upon continuous illumination in the K^+ doped perovskite film, significantly different from the case without K^+ doping. Interface trapping defect density is also significantly reduced by K^+-doping, which increases the hole extraction efficiency and therefore improves the PCE of the perovskite solar cells. We propose that the passivation effect by K^+ doping must be activated by light illumination, after which Br^- anions are bonded with K^+ to form immobile KBr-like compounds as evidenced by STEM measurement. These compounds not only eliminate the mobile halide ion defects in perovskite films but also suppress the ion migration, resulting in improved stability and hysteresis-free PSCs.

2. Results and discussions

The samples used in this study are CsFAMA perovskite thin films with 0 mol% K^+ and 3.5 mol% K^+ doping, hereafter noted as 0mol%K^+ and 3.5mol%K^+ perovskites. The fabrication methods are detailed in the **Experimental Section**[13]. The high uniformity of the 0mol%K^+ and 3.5mol%K^+ perovskite morphologies are demonstrated by the top-view SEM images (Figure S1, Supporting Information (SI)). An enlargement of perovskite grain size is achieved by the 3.5 mol% K^+ doping, ascribed to the accelerated crystallization.[15] The PL and UV-visible absorbance spectra of the 0mol%K^+ and 3.5mol%K^+ perovskites are shown in **Figure** 1**a**. PL spectra of the 0mol%K^+ and 3.5mol%K^+ perovskites both peak at 763 nm. Compared to the 0mol%K^+ perovskite, the absorption

edge for the 3.5mol%K^+ perovskite is only slightly red shifted. According to Tauc equation plot analysis (Figure S2, SI),[24] the bandgap E_g values of the 0mol%K^+ and 3.5mol%K^+ perovskites are 1.591 eV and 1.586 eV, respectively, which implies 3.5 mol% KI incorporation is insufficient to alter the bandgap of CsFAMA perovskite.

To investigate the effect of light illumination on the carrier dynamics in perovskite films, we conducted FLIM characterization for the 0mol%K^+ and 3.5mol%K^+ films under widefield light soaking (bias light). The experimental setup is illustrated in **Figure** 1**b** and detailed in the **Experimental Section**. Note that a 470 nm pulsed laser is used as a probe to acquire FLIM images by scanning across the sample area. With a short dwelling time at each pixel (2 ms), it has a negligible light soaking effect on the perovskite films. To confirm this, we have performed sequential scanning of the identical area without any bias light and found no discernible variation (Figure S3). The continuous light source used for light soaking is a xenon lamp combined with a bandpass filter.

Before light soaking characterization, all perovskite samples were kept in a dark chamber for more than 1 hour to avoid unintended light soaking, and then pristine FLIM images were captured. **Figure 1c-f** are the FLIM image of the non-illuminated pristine 0mol%K^+ perovskite, 0mol%K^+ perovskite/Spiro, 3.5mol%K^+ perovskite and 3.5mol%K^+ perovskite/Spiro film, respectively. Comparing **Figure 1c&e,** the PL intensity of 3.5mol%K^+ perovskite is much higher than that of 0mol%K^+ perovskite with longer PL lifetime, which demonstrates that the 3.5mol%K^+ perovskite film presents fewer nonradiative defects, as discussed in detail later in **Figure 5** and **Figure 6**. Note that by using an NA1.4 oil objective, we can achieve 400 nm spatial resolution FLIM at a PL wavelength of 763 nm,[25] and the grain morphology is distinguishable in the perovskite/Spiro film (**Figure 1d&f**), while uniform PL images are captured in the perovskite-only film (**Figure 1c&e**). This can be ascribed

to the significant lateral diffusion and thus lowered lateral resolution due to the long diffusion length and long lifetime of charge carriers in CsFAMA perovskite.[17] When covered by Spiro, efficient hole extraction dominates the carrier recombination and therefore significantly shortens the PL lifetime,[26] thus the grain morphologies are distinguishable in the FLIM images with grain sizes matching the SEM images (Figure S1).

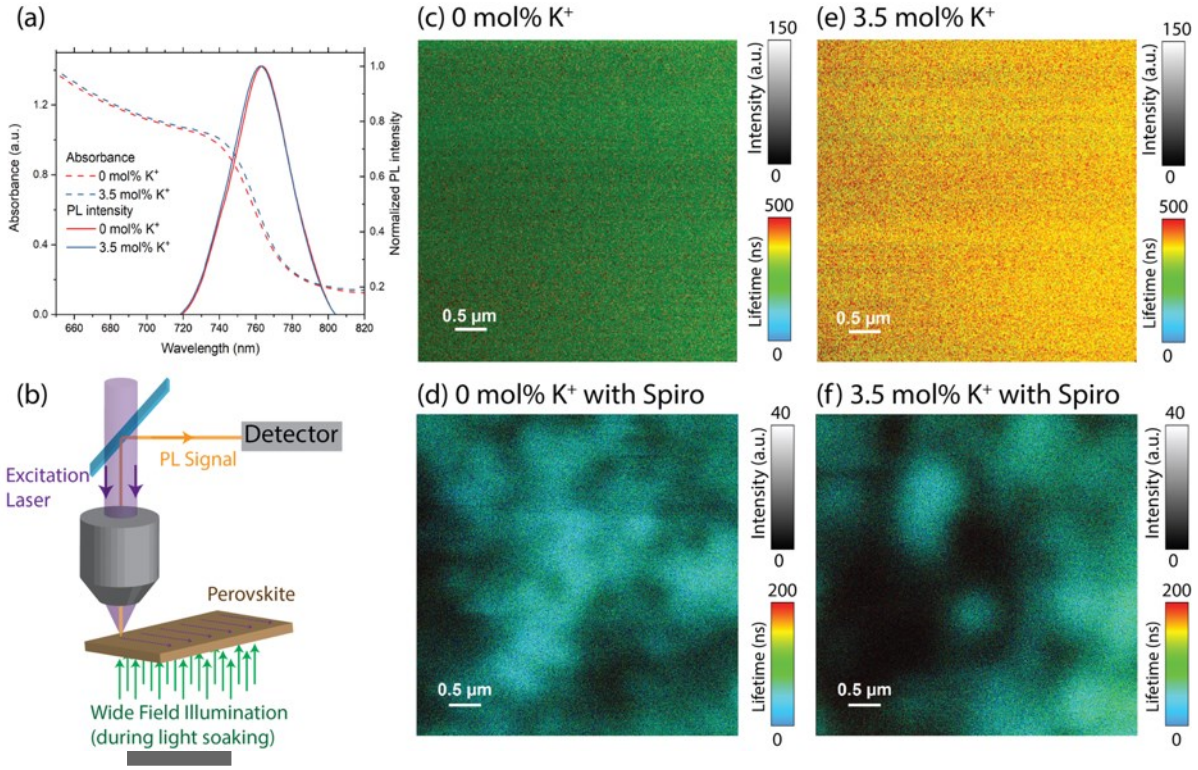

Figure 1. (a) Steady state PL spectra and absorbance of 0mol%K^+ and 3.5mol%K^+ perovskite films; (b) Experimental setup for microscopic PL characterization of perovskite films under bias light soaking; FLIM image of (c) 0mol%K^+ film, (d) 0mol%K^+ perovskite/Spiro, (e) 3.5mol%K^+ film, and (f) 3.5mol%K^+ perovskite/Spiro film in pristine condition.

Figure 2 compares the consecutive FLIM images of 0mol%K^+ and 3.5mol%K^+ perovskites to investigate the impact of light soaking, covering the time periods from the initial dark, bias light ON, and light OFF for recovery. The scanning images of PL intensity (**Figure 2a&b**) and PL lifetime (**Figure**

2**c&d**) are divided into three stages: pre-illumination (Stage 1, pristine condition), illumination light on (Stage 2, light soaking), and post-illumination (Stage 3, dark recovery). The corresponding average PL intensity and photon lifetimes are extracted and plotted as functions of scanning/illumination time (**Figure** 2**e-f**). In the pre-illumination stage (Stage 1), PL intensities obtained from both 0mol%K^+ and 3.5mol%K^+ perovskite films are homogeneously distributed over the whole detected area, as in **Figure** 1**c&e**. During light soaking (Stage 2), the dominant phenomena include the quenching effect of mobile ions activated by light illumination, and an enhancement effect due to defect curing.[27–30] The variations of PL intensity and PL lifetime depend on the competition between these effects. Upon light soaking, the PL intensity of the 0mol%K^+ perovskite film gradually decreases, which is attributed to PL quenching caused by mobile ions activated by light soaking.[27,28] In contrast, the 3.5mol%K^+ perovskite film exhibits a monotonic PL enhancement, ascribed to defect curing during light soaking.[29,30] This is further supported by PL lifetime mapping in **Figure** 2**c&d**. A rapid increase of PL lifetime is observed within the first 100 s of the light soaking period in the 3.5mol%K^+ perovskite, followed by a gradual increase, dominated by light-induced defect curing.

In contrast, the 0mol%K^+ perovskite exhibits a slight increase initially and then undergoes a substantial decrease. In Stage 3, the samples exhibit differing recovery characteristics. With the light off, the PL intensity and lifetime of the 3.5mol%K^+ perovskite exhibits a gradual decrease; while PL intensity of the 0mol%K^+ perovskite recovered, with an intensity increase by 70% after 600 s in the dark, and a slight increase in PL lifetime.

We speculate that, during light soaking, PL quenching in the 0mol%K^+ perovskite is induced by illumination-activated mobile ions.[27,30] In the 3.5mol%K^+ perovskite, PL quenching is significantly suppressed, and defect-curing effects dominate the light soaking process. In contrast, mobile ions

activated during light soaking in the 0mol%K^+ perovskite overwhelms the light-induced defect curing, and therefore leads to a decreased PL intensity and slightly faster PL lifetime. Once returned to the dark, mobile ions dissipate the extra energy and returns the system into an equilibrium,[31] therefore PL intensity of the 0mol%K^+ perovskite recovers. Such competition between defect curing and mobile ion activation during light soaking will be further investigated in detail later in **Figure 5** and **Figure 6**.

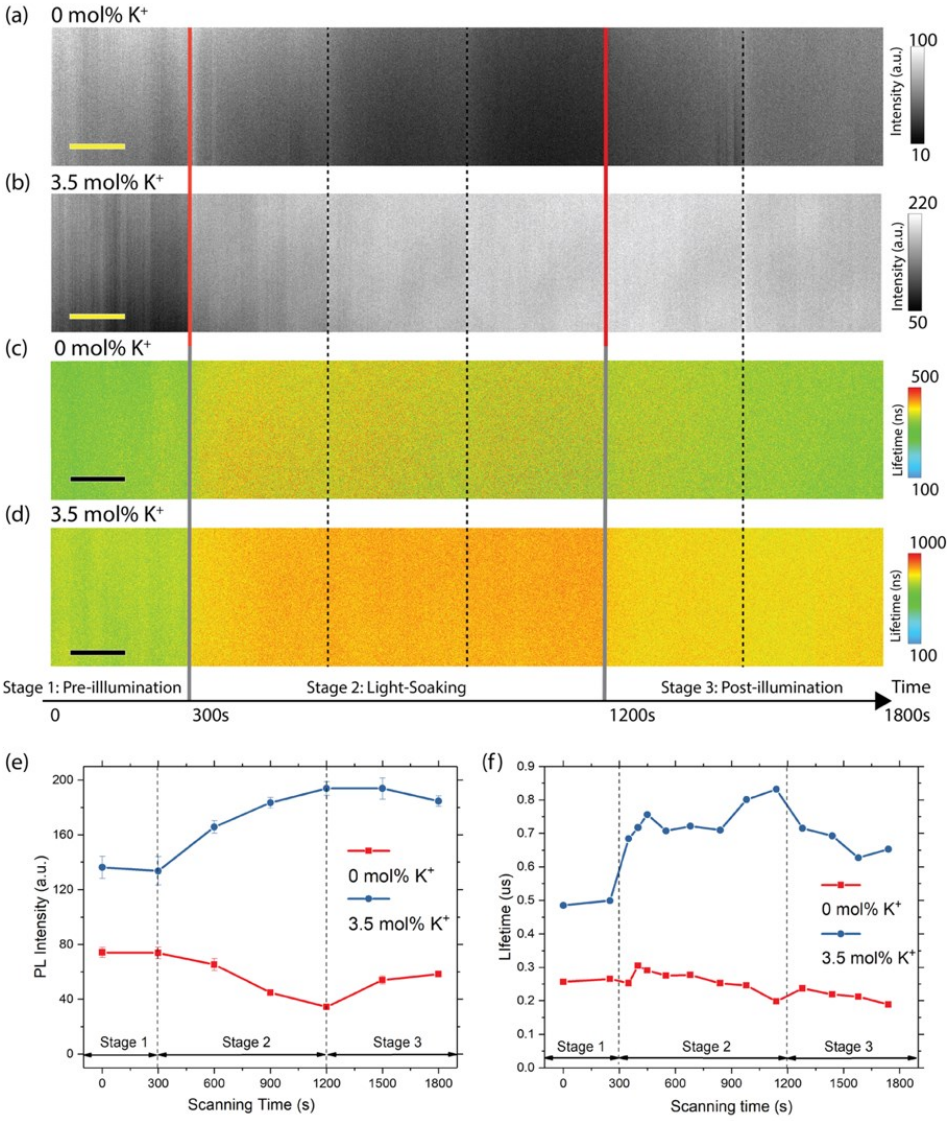

Figure 2. (a-b) PL intensity scanning images of (a) 0mol%K^+ and (b) 3.5mol%K^+ perovskite films; (c-d) PL lifetime scanning images of (c) 0mol%K^+ and (d) 3.5mol%K^+ perovskite films; (e) the corresponding PL intensity versus time plots, and (f) PL lifetime versus time plots. All scale bars represent 1 µm.

The chemical composition of 3.5mol%K^+ perovskite film in a perovskite solar cell device after visible light illumination was investigated by scanning transmission electron microscopy-energy dispersive X-ray spectroscopy (STEM-EDX). **Figure 3a** shows the High-angle annular dark-field (HAADF) image of

the lamella sample (~150 nm in thickness) composed of FTO Glass/SnO_2/Perovskite/Spiro/Pt prepared by lift-off FIB (focused ion beam) technique (see details in **Experimental Section** and Figure S4 in SI)[32]. The Pt layer deposited on the top was used as the mask during ion beam etching. As shown in Figure S4, the compact shape and smooth surface of perovskite lamella obtained indicate that the microstructural change of perovskite film caused by high energy ions does not occur during FIB process in our research. **Figure 3b, c, d** shows the cross-sectional elemental mapping of I, Br, K in the 3.5mol%K^+ perovskite film, respectively. The distribution of I is relatively homogeneous all over the film. In contrast, Br and K have a specific spatial distribution, tracing out the K/Br-rich grains. The similar spatial distribution profile of Br and K highlights the positive correlation between these two elements, which is an unambiguous proof of the formation of KBr-like compounds in 3.5mol%K^+ perovskite film upon light illumination.[20]

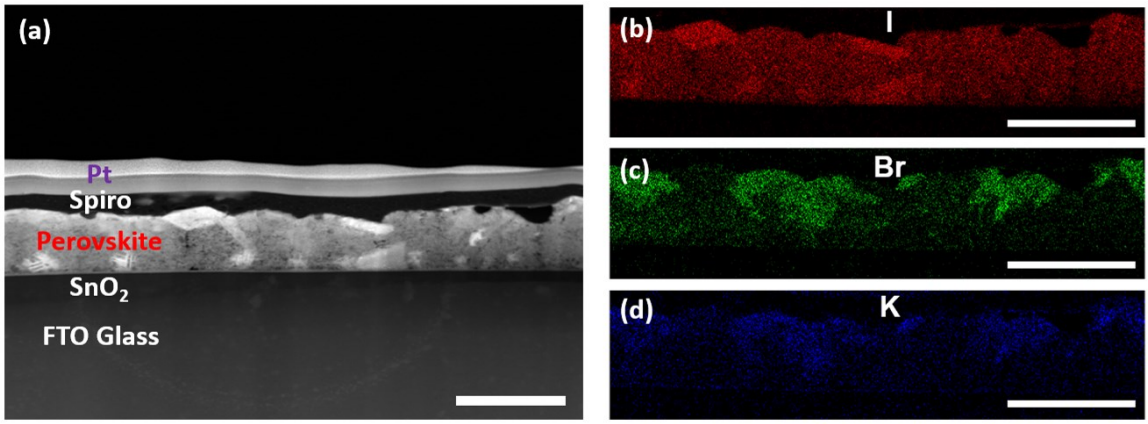

Figure 3. (a) HAADF image of 3.5mol%K^+ perovskite film; (b, c, d) STEM-EDX elemental mapping of I, Br, K in 3.5 mol%K^+ perovskite film. All scale bars represent 1 μm.

It is evidenced that light illumination can induce an improvement in photo-physical properties of the 3.5mol%K^+ perovskite, while in the 0mol%K^+ perovskite light illumination leads to inferior PL

behavior, which is intimately correlated with solar cell performance. **Figure 4a** depicts the device structure of PSCs based on 0mol%K^+ and 3.5mol%K^+ perovskite films with the architecture of FTO/SnO_2/perovskite/Spiro-OMeTAD/Au. The *J-V* curves of PSCs obtained by both forward scan (FS) and reverse scan (RS) are shown in **Figure 4b**, with the corresponding PCE and fill factor (FF) data listed in **Table** 1. The improvement of PCE from 19.26% to 20.25% (reverse scan) upon K^+ doping is similar to our previous reports,[13] demonstrating the improvement of high-performance PSCs by K^+ doping. For the 0mol%K^+ PSC device, FF obtained from the forward scan (0.68) is much smaller than that from the reverse scan (0.77), while the 3.5mol%K^+ PSC shows hysteresis-free behavior with improved steady state PCE.[33] The accuracy of device performance measurements is confirmed by the external quantum efficiency (EQE) spectrum of the PSC measured at short circuit and the corresponding photocurrent integration curve (Figure S5). The steady-state photocurrents of the PSCs measured at the maximum power point (**Figure 4c**) show a much more rapid photo-response for devices based on the 3.5mol%K^+ perovskite compared to the 0mol%K^+ perovskite, indicating an increased performance output stability upon K^+ doping.

To understand the mechanism of this faster and hysteresis-free photocurrent response by 3.5 mol% K^+ doping, lifetime mapping images of 0mol%K^+ perovskite/Spiro and 3.5mol%K^+ perovskite/Spiro films are shown in **Figure 4d,** and the histogram of photon lifetime is plotted in **Figure 4e**. Prior to light soaking, there are two distinct lifetime components observed: a short-lifetime component (peak center around 10 ns) and a long-lifetime component (peak center around 60 ns). Occurrences of the short-lifetime (10 ns) in the 3.5mol%K^+ perovskite/Spiro is distinctly lower than in the 0mol%K^+ perovskite/Spiro, albeit long-lifetime occurrences (60 ns) are similar. The short-lifetime occurrences can be ascribed to defect trapping at the interface between perovskite and Spiro, which

does not appear in the pure perovskite samples. The long-lifetime occurrences originate from the hole extraction by Spiro. The data indicates that interface defect trapping is significantly reduced in the 3.5mol%K^+ perovskite/Spiro film. After light soaking, occurrences of the short-lifetime component disappear, which means that interface trapping can be removed by light soaking. While long-lifetime occurrences were significantly enhanced in both films after light soaking, the overall lifetime in the 3.5mol%K^+ perovskite/Spiro is also shorter than in the 0mol%K^+ perovskite/Spiro, suggesting more efficient hole extraction. These results further confirm that mobile ion activation is suppressed in the 3.5mol%K^+ perovskite, leading to less defect trapping at the perovskite/Spiro interface (fewer short-lifetime occurrences, **Figure 4e**), faster carrier extraction rate (**Figure 4c**), and shortened fundamental PL lifetime (**Figure 4e**).

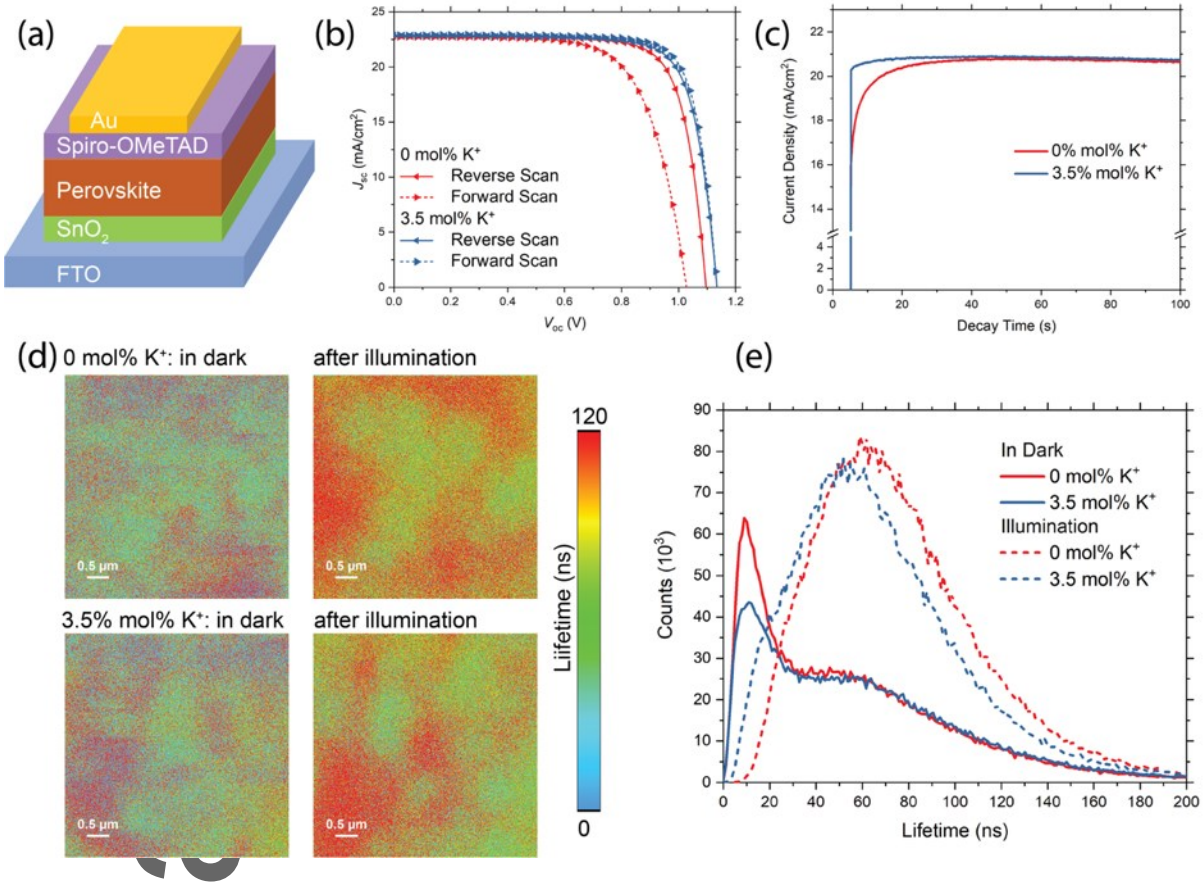

Figure 4. (a) Schematic of perovskite solar cell device structure; (b) J-V characteristic of PSCs based on 0mol%K^+ and 3.5mol%K^+ perovskite films obtained by reverse and forward scan; (c) Steady-state output of photocurrent density measured at the maximum power point under 1 Sun AM 1.5G illumination; (d) PL lifetime scanning images of 0mol%K^+ perovskite/Spiro and 3.5mol%K^+ perovskite/Spiro film in the dark and after illumination; (e) the corresponding distribution of PL lifetime over the measured area in (d).

The decreased defect trapping is further confirmed in the K^+ doped perovskite by ultrafast transient absorption (TA) measurements. **Figure 5a&b** show the pseudo-color representations of the TA spectra (ΔOD: pump-induced change of absorbance) as a function of the probe wavelength and pump-probe delay time for 0mol%K^+ and 3.5mol%K^+ perovskite films, respectively. The main features are the negative ground-state bleaching (GB) with peaks centered at 750 nm, attributed to the depletion of valence band population and associated filling of the conduction band-edge states

by the photoexcited carriers. At longer wavelengths (> 800 nm), a broad but much weaker intensity TA bleaching feature is assigned to the filling of below-gap trap-states.[34] The bleaching decay profiles probed at 850 nm thus reflect the lifetime of carriers trapped in the below-gap defect states, as shown in **Figure 5c**, which is well fitted by a bi-exponential decay function, $I(t) = A_1\exp(-t/\tau_1) + A_1\exp(-t/\tau_1)$, where τ_1 and τ_2 are short and long decay time constants and A_1, A_2 the corresponding weight ratios, summarized in **Table** 2. The average decay constants are calculated by $\tau_a = A_1\tau_1 + A_2\tau_2$, which are 8.9 ± 0.7 ps and 16.6 ± 1.3 ps for 0mol%K^+ and 3.5mol%K^+, respectively. The longer decay time constant of the 3.5mol%K^+ perovskite confirms a lower defect states density (N_t) than 0mol%K^+ perovskite.[34]

To further investigate the illumination effect, PL intensity under a continuous constant excitation is monitored as a function of excitation time for 0mol%K^+ and 3.5mol%K^+ perovskite, as shown in **Figure 5d**, both normalized to the initial PL intensity. The original PL time traces with intensity of photon number are provided in Figure S6, which shows overall higher PL intensity in 3.5mol%K^+ perovskite and confirms a higher PL efficiency by K^+ doping.[35] Both PL time traces exhibit a rapid increase at an early stage, followed by the slow decline at a prolonged timescale. As discussed earlier in **Figure** 2, PL enhancement during light soaking is ascribed to defect curing, while PL quenching is induced by illumination activated mobile ions.[27,30] Under continuous illumination, PL enhancement and PL quenching will eventually reach a dynamic balance state. Therefore, the normalized PL time traces are described as:

$$I(t) = A_{\mathrm{sat}} \cdot \frac{t}{1+t/\tau_{\mathrm{sat}}} - A_{\mathrm{exp}} \cdot \left[1 - exp\left(\frac{-t}{\tau_{\mathrm{exp}}}\right)\right] \quad (1)$$

where τ_{sat} and τ_{exp} are the time constants, A_{sat} and A_{exp} the corresponding weight ratios. The first part (a saturation function) describes the PL enhancement by defects curing[30] and the second part, which is an exponential quenching function, describes PL quenching by light-activated mobile ions.[30,36] All the fitting parameters are summarized in **Table** 3, and the saturation and the quenching curves are separately plotted in **Figure 5e** for both 0mol%K^+ and 3.5mol%K^+ perovskite. The curves of PL enhancement are similar in 0mol%K^+ and 3.5mol%K^+ perovskite films, indicating the similar effect of light-induced defect curing in both cases. Regarding the quenching component, the fitting gives significantly different time constants (τ_{exp}) of 137s and 294s for 0mol%K^+ and 3.5mol%K^+ perovskite, respectively. Since PL quenching during light soaking is ascribed to the accumulation of ionized halide anions,[27] the slower PL decline in 3.5mol%K^+ perovskite implies the activation of mobile ions are suppressed, therefore resulting in an improved photostability and better PCE performance.

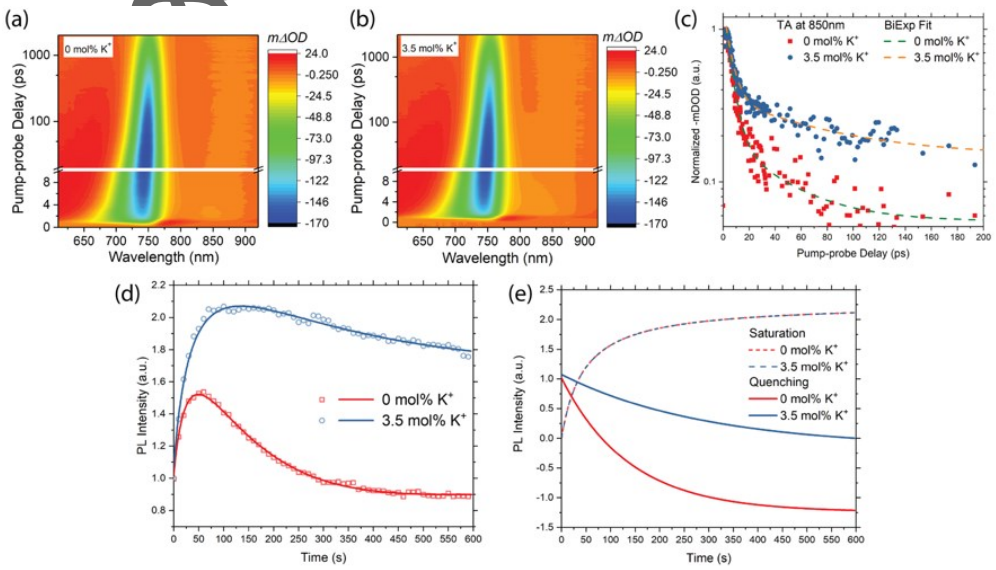

Figure 5. Two-dimensional pseudo-color TA spectra (ΔOD) as a function of probe wavelength and pump-probe delay time for (a) 0mol%K^+ perovskite and (b) 3.5mol%K^+ perovskite; (c) Normalized kinetic decay profiles detected at 850 nm for 0mol%K^+ and 3.5mol%K^+ perovskites; (d) Normalized PL intensity time traces and corresponding fitting

curves for 0mol%K^+ and 3.5mol%K^+ perovskite films upon continuous excitation; (e) Separated PL increase and decrease components of 0mol%K^+ and 3.5mol%K^+ perovskites.

Figure 6a&b shows the normalized PL spectral evolution of 0mol%K^+ and 3.5mol%K^+ perovskite films during the continuous excitation. The PL spectra of 0mol%K^+ perovskite (**Figure 6a**) remain stable with continuous excitation, without significant wavelength shift or variation of full width at half maximum (FWHM). By contrast, **Figure 6b** shows that the PL spectra of the 3.5mol%K^+ perovskite undergo a broadening of FWHM and redshift of peak wavelength with increasing excitation time. Such broadening of the PL spectra might be ascribed to the increased diversity of optical band states induced by perovskite compositional change during continuous excitation. **Figure 6c** summarizes the shifting profiles of PL peak positions of both 0mol%K^+ and 3.5mol%K^+ perovskite for comparison. Initially, the peak positions of both perovskite films are around 763 nm (1.63 eV). With longer excitation times, the PL peak in the 0mol%K^+ perovskite redshifts only slightly to 764 nm, while in the 3.5mol%K^+ perovskite film a substantial redshift to 769 nm (1.61 eV) is observed. It should be noted that the redshift in the K^+ doped perovskite caused by light soaking is irreversible and much smaller (6 nm or 20 meV). Therefore, phase segregation[37,38] due to halide exchange is unlikely to be the mechanism. It has been elucidated that K^+ does not incorporate into the perovskite lattice.[16] Instead, we speculate that the bandgap of the K^+ doped perovskite is slightly disturbed due to halide substitution of bromide ions (Br^-) by the excess iodide ions (I^-) in the grain boundary. We proposed that "I^- to Br^-" halide substitution process in the K^+ doped sample is triggered by light illumination upon which halide ions are activated for ion exchange, facilitated by the formation of stable KBr-like compunds at grain boundaries which suppresses the inverse "Br^- to I^-" substitution. This interpretation is consistent with previous explanations in potassium doped mixed halide (I/Br)

perovskites that KBr has a stronger ionic bond compared to KI.[20,21,23] Without the presence of K^+ ions, as in the case of 0mol%K^+ case, minor halide substitution leads to the steady PL peak.

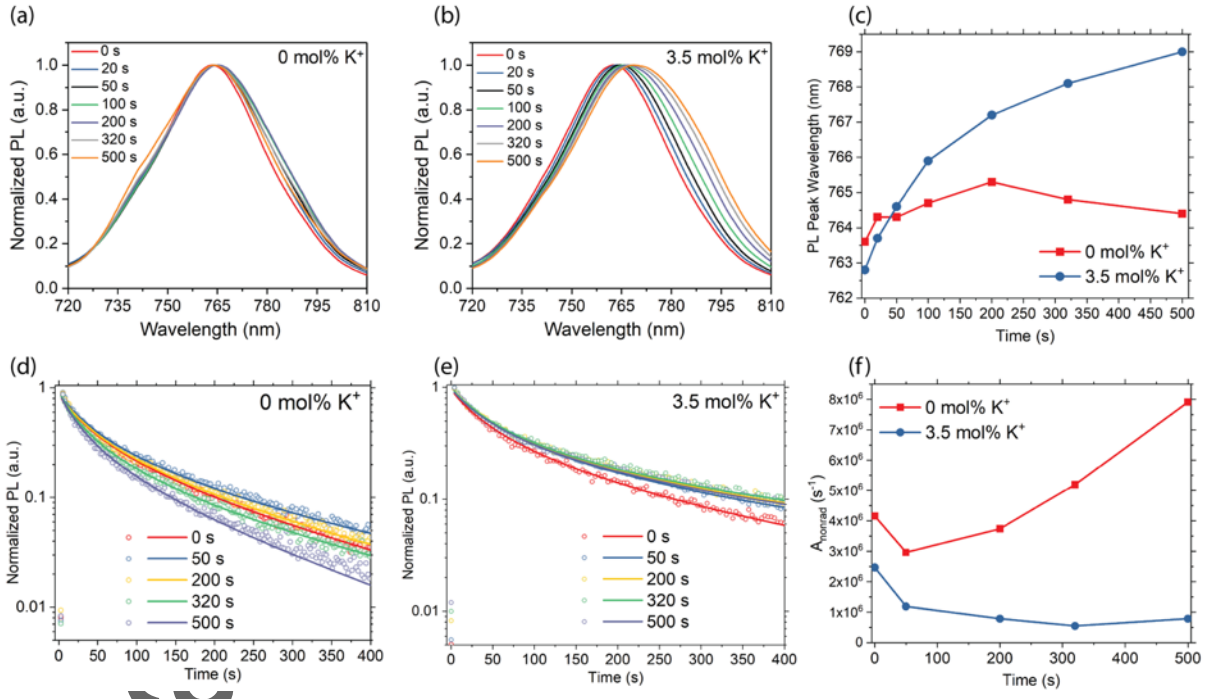

Figure 6. PL spectra at various excitation time for (a) 0mol%K^+ perovskite and (b) 3.5mol%K^+ perovskite; (c) PL peak positions of 0mol%K^+ and 3.5mol%K^+ perovskite films plotted to excitation time; TRPL decay profiles and corresponding fitting curves of (d) 0mol%K^+ perovskite film and (e) 3.5mol%K^+ perovskite film under various consecutive excitation time; (f) Fitted nonradiative defect trapping coefficient of 0mol%K^+ , and 3.5mol%K^+ perovskites plotted versus the excitation time.

Time-resolved PL (TRPL) of perovskite films in 0mol%K^+ and 3.5mol%K^+ perovskite was measured at various excitation time during continuous excitation, as shown in **Figure 6d**&**e**. The PL decay profiles of the 0mol%K^+ perovskite become slower during initial illumination (0-50 s), followed by a dramatically faster decay under prolonged illumination (200-500 s). For the 3.5mol%K^+ sample, the PL decay profile monotonously evolves to slower decay behaviors after continuous illumination. In this work, Auger recombination is ignored due to the low excitation intensity (160 nJ/cm^2) adopted

and low Auger coefficient in perovskite.[39] Therefore, time-resolved carrier density ($n(t)$) and PL intensity ($I_{PL}(t)$) can be described as:

$$\frac{dn(t)}{dt} = -A \cdot n(t) - B \cdot n(t)^2 \quad \text{(2-a)}$$

$$I_{PL}(t) \propto B \cdot n(t)^2 + B \cdot m_0 \cdot n(t) \quad \text{(2-b)}$$

where *A* and *B* are the coefficients of defect trapping and electron-hole recombination, respectively, and m_0 is the unintentionally doped carrier density in perovskite.[40] Solving equations 2a-b, the PL intensity $I(t)$ as a function of time delay after excitation can be expressed as:

$$I_{\mathrm{PL}}(t) \propto \left(\frac{exp(-At)}{1+\frac{N_0 B}{A}(1-exp(-At))}\right)^2 + M_0 \cdot \left(\frac{exp(-At)}{1+\frac{N_0 B}{A}(1-exp(-At))}\right) \quad \text{(3)}$$

N_0 is the initial carrier density estimated to be 3×10^{16} cm^{-3} according to $N_0 = A_\lambda \cdot F/(E_{\mathrm{ph}} \cdot d)$, where A_λ is the absorbance at 405 nm, E_{ph} is the photon energy, F is the excitation fluence and d is the film thickness.[41] Global fitting based on Equation (3) is applied to all decay curves where *B* is set to be 6.7×10^{-10} cm^3/s as per the results of Yamada et al.[42] Non-radiative defect trapping coefficients *A* for both 0mol%K^+ and 3.5mol%K^+ samples under various illumination time are acquired and plotted in **Figure 6f**, which reflect the trap (defect) states density.[43] At the beginning of illumination (*t* = 0 s), the defect trapping coefficient of carriers in 0mol%K^+ perovskite film (4.2×10^6 s^{-1}) is about 2 times higher than that obtained from the 3.5mol%K^+ sample (2.4×10^6 s^{-1}), which is consistent with the decreased defect state density upon K^+ doping revealed by the TA characterization (**Figure 5a-c**). The decreased *A* values for both samples at the initial stage of illumination can be assigned to the light induced defect curing process as in the discussion of **Figure 5d**&**e**. The *A* for the 0mol%K^+ perovskite increases significantly under prolonged illumination, finally reaching 7.9×10^6 s^{-1} at *t* = 500 s, and is ascribed to the appearance of light activated mobile halide

ions acting as the new trap states. In contrast, the value of *A* for the 3.5mol%K^+ perovskite monotonously decreases to 7.8×10^5 s^{-1}, ascribed to the suppression of light activated mobile ions due to the formation of strong bonded KBr-like compounds.

In **Figure 7**, our mechanism for the role of K^+ for the passivation of mixed cation lead mixed halide perovskite is schematically illustrated. In 0mol%K^+ perovskite (CsFAMA), defects trapping at the interface between the perovskite and Spiro impedes hole extraction and lowers the PCE (**Figure 7a & 4b**). While such interface trapping can be gradually passivated during light soaking (**Figure 7b**), the doping of 3.5mol%K^+ significantly reduces the interface defect density and improves the solar cell PCE (**Figure 7c**). What is more, when 0mol%K^+ perovskite is continuously illuminated (**Figure 7b**), halide ions are photo-activated, and the corresponding halide vacancies become mobile, which are responsible for the PL quenching during light soaking (**Figure** 2**a&c** and **Figure 5d&e**) and the hysteresis in PSC devices (**Figure 4b**).[44] In contrast, hysteresis and light-induced PL quenching in the 3.5mol%K^+ perovskite is significantly suppressed, where the passivation effect by K^+ doping is triggered by illumination. In the dark state, K^+ located in film surface and grain boundaries are loosely bound to I^- or in the unbound state (**Figure 7c**). Upon illumination, photo-activated mobile ions are stabilized by the formation of KBr-like compounds. The presence of KBr compounds at grain boundaries/surfaces in K^+ doped perovskite has been previously proposed by the Stranks group [20] and later confirmed by the Gratzel group using ^{39}K solid-state NMR.[23] The STEM result (**Figure 3**) in this work also indicates the presence of KBr-like compounds in K^+ doped perovskite film sample upon light illumination. Therefore, illumination triggered KBr-like compounds formation at grain boundaries is unambiguously adopted to interpret our results which decrease the number of mobile halide ions and suppress ion migration in the working devices. Additionally, the formation of KBr-like

compounds facilitates homogeneous halide substitution (Br^- substituted by I^-) in perovskite phase, as shown by the redshift of the PL peak in **Figure 6b** and longer PL lifetime in **Figure 2d** during light soaking. Unlike phase segregation in hybrid halide perovskites without K^+ doping,[45] such halide substitution is irreversible. Therefore, once triggered by illumination, K^+ doped perovskite retains the superior passivation effect even after being placed back in the dark. Here we would like to emphasize that light illumination is essential to trigger the passivation effect of K^+ doping in mixed-cation lead mixed-halide perovskite materials not only by confining the mobile ion, but also by reducing the interface trapping defect density, resulting in improved performance of the PSCs.

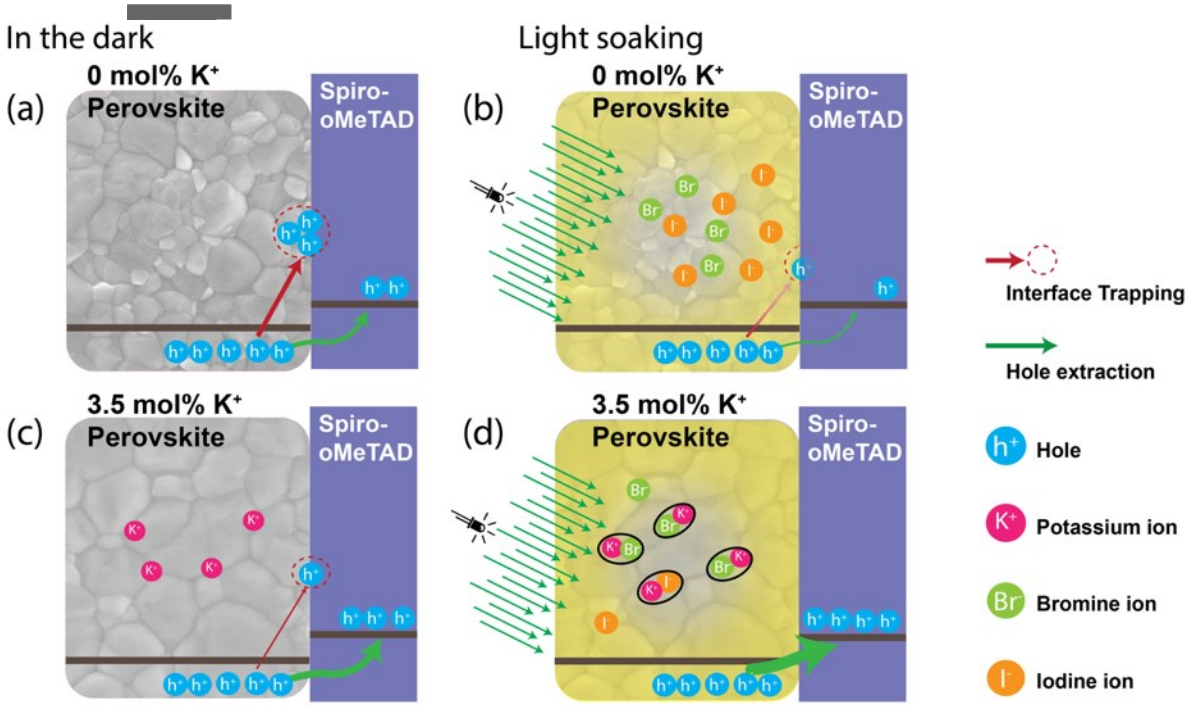

Figure 7. Schematic of the passivation effect of K^+ doped perovskite triggered by illumination: (a-b) 0mol%K^+ perovskite & (c-d) 3.5mol%K^+ perovskite in the dark and during light soaking, respectively.

3. Conclusion

In summary, we have performed time-dependent and time-resolved PL, together with PL lifetime mapping and transient absorption, on the mixed-cation mixed-halide perovskite ($Cs_{0.05}(FA_{0.85}MA_{0.15})_{0.95}Pb(I_{0.85}Br_{0.15})_3$) films both with or without an optimal 3.5 mol% potassium (K^+) doping. We confirmed that illumination-triggered passivation is occurring in the K^+ doped perovskite, which is responsible for the improved PSC performance, exhibited by higher PCE and negligible hysteresis. Therefore, it is proposed that illumination facilitates the formation of stable KBr-like compounds in the K^+ doped perovskite film, which is consistent with the earlier reported results and provides further insights into the doped K^+ dynamics during illumination. K^+ doping of perovskite films effectively reduces the interface trapping defect density and suppresses ion migration. Together with the formation of KBr-like compounds, homogeneous and irreversible halide substitution also takes place under illumination, which is vital to retaining the superior passivation effect of K^+ doping. This highlights the critical role of light illumination in triggering the passivation effect of K^+ doping in perovskite materials to achieve hysteresis-free PSCs with long-term stability. This work provides in-depth insight into this mechanism and is of crucial importance for understanding the working principle and to improve the design of perovskite-based devices.

Table 1. The performance parameters of PSCs based on 0mol%K^+ and 3.5mol%K^+ perovskite

	Sweep	VOC (V)	JSC (mA/cm^2)	FF	PCE	Integrated J_{SC} (mA/cm^2)
0mol%K^+	Forward	1.028	22.72	0.68	15.88	22.43
	Reverse	1.097	22.77	0.77	19.26	
3.5mol%K^+	Forward	1.135	22.84	0.79	20.58	22.58
	Reverse	1.135	22.88	0.78	20.25	

Table 2. Fitting parameters of TA kinetic decay at 850 nm.

	A_1	τ_1 (ps)	A_2	τ_1 (ps)	τ_a (ps)
0mol%K^+	0.896	5.2±0.3	0.104	41±5	8.9±0.7
3.5mol%K^+	0.836	5.5±0.2	0.164	73±7	16.6±1.3

Table 3. Fitting parameters of PL saturation and exponential quenching functions

	A_{sat}	$\tau_{\mathrm{sat}}(s)$	A_{exp}	$\tau_{\mathrm{exp}}(s)$
0mol%K^+	0.050±0.001	45.0±0.3	1.24±0.01	137.4±0.12
3.5mol%K^+	0.044±0.001	43.6±0.5	0.161±0.008	294.0±2.50

Experimental Section

Materials

$SnCl_2 \bullet 2H_2O$ was purchased from Aladdin Industrial Corporation (Shanghai, China). Formamidinium iodide (FAI) and methylammonium bromine (MABr) were purchased from Lumtec, Taiwan. Lead iodide (PbI_2) and lead bromine ($PbBr_2$) were purchased from TCI. CsI and KI were purchased from Sigma-Aldrich. Spiro-OMeTAD was purchased from Shenzhen Feiming Science and Technology Co., Ltd. All these chemicals were used as received without further purification.

Film Preparation

The preparation of mixed-perovskite precursor solutions without and with K doping: the $Cs_{0.05}(FA_{0.85}MA_{0.15})_{0.95}Pb(I_{0.85}Br_{0.15})_3$ (CsFAMA) perovskite precursor was prepared by mixing 2.0 M CsI solution, 1.3 M organic salts solution (FAI: MABr = 0.85:0.15), and 1.4 M metal lead salts (PbI_2: $PbBr_2$ = 0.85:0.15) solution in the DMF/DMSO (4:1) with the volume ratio of 3.3:95:95; the precursor solution of KCsFAMA perovskite with 3.5 mol% molar ratio K^+ doping was prepared by adding relatively 2.3 vol.% of 2.0 M KI solution (DMSO) into the Cs/FA/MA perovskite precursor.

25 µL of precursor solution was spun at 6000 rpm for 30 s with an accelerated speed of 1000 rpm in a N_2 filled glove box, followed by 100 µL anti-solvents of ethyl acetate dropped at the last 5 seconds. After annealed at 120 °C for 45 min, the films were encapsulated with coverslip glasses contacting the topside, connected by epoxy glue on the surrounding edge.

For the PSC device fabrication, the compact SnO_2 electron transporting layer was firstly deposited on cleaned FTO substrate from diluted $SnCl_2 \bullet 2H_2O$ aqueous solution (0.002 M) by chemical bath deposition (CBD) method. Mixed-perovskite film was then spin-coated onto SnO_2 layer using parameters aforementioned. After annealing, 25 µL Spiro-OMeTAD solution was spun on the mixed-perovskite film at 3000 rpm for 30 s. Finally, 60 nm of gold layer was evaporated on the top of Spiro as the back electrode to complete the whole PSC device with the architecture of FTO/SnO_2/Mixed-perovskite/Spiro/Au.

General Characterizations

SEM: The surface morphologies of the perovskite films and cross-sectional structure of the perovskite solar cells were investigated using a field-emission scanning electron microscopy (FESEM, Zeiss Ultra Plus).

STEM: The lamella sample of perovskite film with the structure of FTO/SnO2/Mixed-perovskite/Spiro was prepared on a FEI Tecnai F30 at the Bio21 Advanced Microscopy Facility by a focused ion beam (FIB). A Pt (platinum) bar was firstly deposited on the surface of sample film acting as the mask. After ion beam etching, the lamella was lifted-off and transfered to the copper grid. Several cycles of gentle milling was applied to finally obtain a cross-section lamella with 150 nm thickness (as illustrated in Figure S4, SI). The HAADF image and STEM-EDX elemental mapping of 3.5 mol%K^+

perovskite cross-sectional film were obtained by a FEI Tecnai F20 high resolution transmission electron microscope.

Devices performance

The photocurrent density-voltage (J-V) curves of the PSCs based on mixed-perovskites w/o and with K^+ doping were measured using a solar simulator (Oriel 94023A, 300 W) to provide 0.1 W/cm^2 sun-light illumination and a Keithley 2400 source meter for data collection. Both forward scan (from -0.1 V to 1.2 V) and reverse scan (from 1.2 V to -0.1 V) were conducted for each device with scanning rate of 100 mV/s.

UV-Vis & TA

UV-visible spectra were obtained with UV/VIS/NIR Spectrometer (Lambda 1050, Perkin Elmer). Femtosecond pump-probe transient absorption (TA) measurements for all film samples were performed using a TA spectrometer at room temperature. Briefly, a Ti:sapphire mode-locked oscillator seeded a regenerative amplifier (Spitfire Pro XP 100F, Spectra Physics) to generate 800 nm laser pulses with a 1 kHz repetition rate and 100 fs pulse duration, and was split into two paths to generate the pump and probe beams. The 400 nm pump beam was produced by frequency-doubling using a BBO crystal. The white-light super-continuum probe beam was generated in a 3.2 mm sapphire crystal seeded by the 1200 nm signal of a optical parametric amplifier (TOPAS-C, Light Conversion). The pump beam was focused on to the sample surface with a FWHM spot size of 880 µm and a 90 µJ/cm^2 fluence. The FWHM spot size of the probe beam was 120 µm and had a power much lower than the pump. The transmitted probe beam was detected by a polychromatic-CCD.

Photoluminescence Measurements

A 405 nm pulsed laser was used as the excitation for steady state photoluminescence (PL) measurements. The excitation beam was focused to the sample with the beam area of 1 μm^2 by an objective and the pulse fluence was attenuated to 160 nJ/cm^2 by a neutral density filter. PL signals were collected in the reflection mode by the same objective and focused onto an optical fiber coupled spectrometer equipped with a CCD. The PL intensity was recorded as a function of illumination time (PL time-trace) under continuous constant illumination, by connecting the optical fiber to a TCSPC module (PicoHarp 300) for time correlated single photon counting (TCSPC) analysis. The TCSPC measurements were carried out at selected times (0 s, 50 s, 200 s, 320 s, 500 s) after the excitation illumination started and took 10 s for integral.

The FLIM were conducted by a confocal laser scanning microscopy coupled with TCSPC module (MT200, Picoquant), **Figure 1b**. A 470 nm pulsed laser with a repetition rate of 1 MHz was used as excitation light focused on the front side of the perovskite film. At the same time, the sample film was continuously illuminated (wide field, light soaking, 70 mW/cm^2) on the back side (glass side) through a 525/50 nm band-pass filter. Fluorescence signal emitted from the front side was detected through a 760/40 nm band-pass filter which blocked both excitation light and soaking light. The scanning mode is point by point from left to right and line by line from top to bottom (**Figure** 1 & **Figure 3**). FLIM images in **Figure** 2 are rotated by 90° and joint together according to scanning sequence, therefore demonstrating the PL dynamic under continuous illumination. FLIM collection at each point took 2 ms. The total collection time to full FLIM image of a 5 µm × 5 µm area was 300 s.

Supporting Information

Supporting Information is available from the Wiley Online Library or from the author.

Acknowledgements

F. Zheng and W. Chen contributed equally to this work. B. Jia acknowledges support from the Australia Research Council through the Discovery Project scheme (DP150102972, DP190103186) and Industrial Transformation Training Centres scheme (IC180100005). F. Zheng and K. P. Ghiggino thank the Australian Research Council for support under Grant CE170100026. Dr. Sergey Rubanov is acknowledged for the assistance of STEM-EDX measurement carried out at the Bio21 Advanced Microscopy Facility.

Received: ((will be filled in by the editorial staff))
Revised: ((will be filled in by the editorial staff))
Published online: ((will be filled in by the editorial staff))

References

[1] M. A. Green, A. Ho-Baillie, H. J. Snaith, *Nat. Photonics* **2014**, *8*, 506.

[2] H. J. Snaith, *Nat. Mater.* **2018**, *17*, 372.

[3] T. Bu, J. Li, F. Zheng, W. Chen, X. Wen, Z. Ku, Y. Peng, J. Zhong, Y. B. Cheng, F. Huang, *Nat. Commun.* **2018**, *9*, 1.

[4] Z. Gan, X. Wen, W. Chen, C. Zhou, S. Yang, G. Cao, K. P. Ghiggino, H. Zhang, B. Jia, *Adv. Energy Mater.* **2019**, *1900185*, 1900185.

[5] A. Kojima, K. Teshima, Y. Shirai, T. Miyasaka, *J. Am. Chem. Soc.* **2009**, *131*, 6050.

[6] NREL, NREL. Efficiency Chart. **2020**.

[7] D. P. McMeekin, G. Sadoughi, W. Rehman, G. E. Eperon, M. Saliba, M. T. Horantner, A. Haghighirad, N. Sakai, L. Korte, B. Rech, M. B. Johnston, L. M. Herz, H. J. Snaith, *Science (80-.).* **2016**, *351*, 151.

[8] G. Longo, C. Momblona, M.-G. La-Placa, L. Gil-Escrig, M. Sessolo, H. J. Bolink, *ACS Energy Lett.* **2018**, *3*, 214.

[9] M. Saliba, T. Matsui, J. Y. Seo, K. Domanski, J. P. Correa-Baena, M. K. Nazeeruddin, S. M. Zakeeruddin, W. Tress, A. Abate, A. Hagfeldt, M. Gratzel, *Energy Env. Sci* **2016**, *9*, 1989.

[10] M. Saliba, T. Matsui, K. Domanski, J.-Y. Seo, A. Ummadisingu, S. M. Zakeeruddin, J.-P. Correa-Baena, W. R. Tress, A. Abate, A. Hagfeldt, M. Gratzel, *Science.* **2016**, *354*, 206.

[11] T. J. Jacobsson, S. Svanström, V. Andrei, J. P. H. Rivett, N. Kornienko, B. Philippe, U. B. Cappel, H. Rensmo, F. Deschler, G. Boschloo, *J. Phys. Chem. C* **2018**, *122*, 13548.

[12] S.-H. Turren-Cruz, M. Saliba, M. T. Mayer, H. Juárez-Santiesteban, X. Mathew, L. Nienhaus, W. Tress, M. P. Erodici, M.-J. Sher, M. G. Bawendi, M. Grätzel, A. Abate, A. Hagfeldt, J.-P. Correa-

Baena, *Energy Environ. Sci.* **2018**, *11*, 78.

[13] T. Bu, X. Liu, Y. Zhou, J. Yi, X. Huang, L. Luo, J. Xiao, Z. Ku, Y. Peng, F. Huang, Y. B. Cheng, J. Zhong, *Energy Environ. Sci.* **2017**, *10*, 2509.

[14] D. Yao, C. Zhang, N. D. Pham, Y. Zhang, V. T. Tiong, A. Du, Q. Shen, G. J. Wilson, H. Wang, *J Phys Chem Lett* **2018**, *9*, 2113.

[15] M. R. Filip, G. E. Eperon, H. J. Snaith, F. Giustino, *Nat Commun* **2014**, *5*, 5757.

[16] D. J. Kubicki, D. Prochowicz, A. Hofstetter, S. M. Zakeeruddin, M. Gratzel, L. Emsley, *J Am Chem Soc* **2018**, *140*, 7232.

[17] W. Rehman, D. P. McMeekin, J. B. Patel, R. L. Milot, M. B. Johnston, H. J. Snaith, L. M. Herz, *Energy Environ. Sci.* **2017**, *10*, 361.

[18] Y. Zhang, G. Grancini, Y. Feng, A. M. Asiri, M. K. Nazeeruddin, *ACS Energy Lett.* **2017**, *2*, 802.

[19] J. Cao, S. X. Tao, P. A. Bobbert, C.-P. Wong, N. Zhao, *Adv. Mater.* **2018**, *30*, 1707350.

[20] M. Abdi-Jalebi, Z. Andaji-Garmaroudi, S. Cacovich, C. Stavrakas, B. Philippe, J. M. Richter, M. Alsari, E. P. Booker, E. M. Hutter, A. J. Pearson, S. Lilliu, T. J. Savenije, H. Rensmo, G. Divitini, C. Ducati, R. H. Friend, S. D. Stranks, *Nature* **2018**, *555*, 497.

[21] T. Bu, J. Li, F. Zheng, W. Chen, X. Wen, Z. Ku, Y. Peng, J. Zhong, Y.-B. Cheng, F. Huang, *Nat. Commun.* **2018**, *9*, 4609.

[22] X. Tang, M. van den Berg, E. Gu, A. Horneber, G. J. Matt, A. Osvet, A. J. Meixner, D. Zhang, C. J. Brabec, *Nano Lett.* **2018**, *18*, 2172.

[23] D. J. Kubicki, D. Prochowicz, A. Hofstetter, S. M. Zakeeruddin, M. Grätzel, L. Emsley, *J. Am. Chem. Soc.* **2018**, jacs. 8b03191.

[24] F. Zheng, W.-L. Xu, H.-D. Jin, X.-T. Hao, K. P. Ghiggino, *RSC Adv.* **2015**, *5*, 89515.

[25] W. Chen, X. Wen, M. Latzel, M. Heilmann, J. Yang, X. Dai, S. Huang, S. Shrestha, R. Patterson, S. Christiansen, *ACS Appl. Mater. Interfaces* **2016**, *8*, 31887.

[26] F. Zheng, X. Wen, T. Bu, S. Chen, J. Yang, W. Chen, F. Huang, Y.-B. Cheng, B. Jia, *ACS Appl. Mater. Interfaces* **2018**, *10*, acsami.8b13932.

[27] X. Wen, A. Ho-Baillie, S. Huang, R. Sheng, S. Chen, H. Ko, M. A. Green, *Nano Lett.* **2015**, *15*, 4644.

[28] C. Eames, J. M. Frost, P. R. F. Barnes, B. C. O'Regan, A. Walsh, M. S. Islam, *Nat. Commun.* **2015**, *6*, 7497.

[29] E. Mosconi, D. Meggiolaro, H. J. Snaith, S. D. Stranks, F. De Angelis, *Energy Environ. Sci.* **2016**, *9*, 3180.

[30] S. Chen, X. Wen, S. Huang, F. Huang, Y.-B. Cheng, M. Green, A. Ho-Baillie, *Sol. RRL* **2017**, *1*.

[31] A. J. Barker, A. Sadhanala, F. Deschler, M. Gandini, S. P. Senanayak, P. M. Pearce, E. Mosconi, A. J. Pearson, Y. Wu, A. R. Srimath Kandada, T. Leijtens, F. De Angelis, S. E. Dutton, A. Petrozza, R. H. Friend, *ACS Energy Lett.* **2017**, *2*, 1416.

[32] F. Huang, Y. Dkhissi, W. Huang, M. Xiao, I. Benesperi, S. Rubanov, Y. Zhu, X. Lin, L. Jiang, Y. Zhou, A. Gray-Weale, J. Etheridge, C. R. McNeill, R. A. Caruso, U. Bach, L. Spiccia, Y. B. Cheng,

Nano Energy **2014**, *10*, 10.

[33] S. N. Habisreutinger, N. K. Noel, H. J. Snaith, *ACS Energy Lett.* **2018**, 2472.

[34] X. Wu, M. T. Trinh, D. Niesner, H. Zhu, Z. Norman, J. S. Owen, O. Yaffe, B. J. Kudisch, X. Y. Zhu, *J Am Chem Soc* **2015**, *137*, 2089.

[35] M. Abdi-Jalebi, Z. Andaji-Garmaroudi, S. Cacovich, C. Stavrakas, B. Philippe, J. M. Richter, M. Alsari, E. P. Booker, E. M. Hutter, A. J. Pearson, S. Lilliu, T. J. Savenije, H. Rensmo, G. Divitini, C. Ducati, R. H. Friend, S. D. Stranks, *Nature* **2018**, *555*, 497.

[36] X. Deng, X. Wen, S. Huang, R. Sheng, T. Harada, T. W. Kee, M. Green, A. Ho-Baillie, *J. Phys. Chem. C* **2016**, *120*, 2542.

[37] E. T. Hoke, D. J. Slotcavage, E. R. Dohner, A. R. Bowring, H. I. Karunadasa, M. D. McGehee, *Chem. Sci.* **2015**, *6*, 613.

[38] S. J. Yoon, S. Draguta, J. S. Manser, O. Sharia, W. F. Schneider, M. Kuno, P. V. Kamat, *ACS Energy Lett.* **2016**, *1*, 290.

[39] X. Wen, W. Chen, J. Yang, Q. Ou, T. Yang, C. Zhou, H. Lin, Z. Wang, Y. Zhang, G. Conibeer, Q. Bao, B. Jia, D. J. Moss, *ACS Appl. Mater. Interfaces* **2018**, *10*, 31586.

[40] T. Handa, D. M. Tex, A. Shimazaki, A. Wakamiya, Y. Kanemitsu, *J Phys Chem Lett* **2017**, *8*, 954.

[41] J. Yang, X. Wen, H. Xia, R. Sheng, Q. Ma, J. Kim, P. Tapping, T. Harada, T. W. Kee, F. Huang, Y.-B. Cheng, M. Green, A. Ho-Baillie, S. Huang, S. Shrestha, R. Patterson, G. Conibeer, *Nat. Commun.* **2017**, *8*, 14120.

[42] Y. Yamada, T. Nakamura, M. Endo, A. Wakamiya, Y. Kanemitsu, *J. Am. Chem. Soc.* **2014**, *136*, 11610.

[43] S. D. Stranks, V. M. Burlakov, T. Leijtens, J. M. Ball, A. Goriely, H. J. Snaith, *Phys. Rev. Appl.* **2014**, *2*, 1.

[44] C. Li, S. Tscheuschner, F. Paulus, P. E. Hopkinson, J. Kießling, A. Köhler, Y. Vaynzof, S. Huettner, *Adv. Mater.* **2016**, *28*, 2446.

[45] M. C. Brennan, S. Draguta, P. V. Kamat, M. Kuno, *ACS Energy Lett.* **2018**, *3*, 204.

The table of contents entry

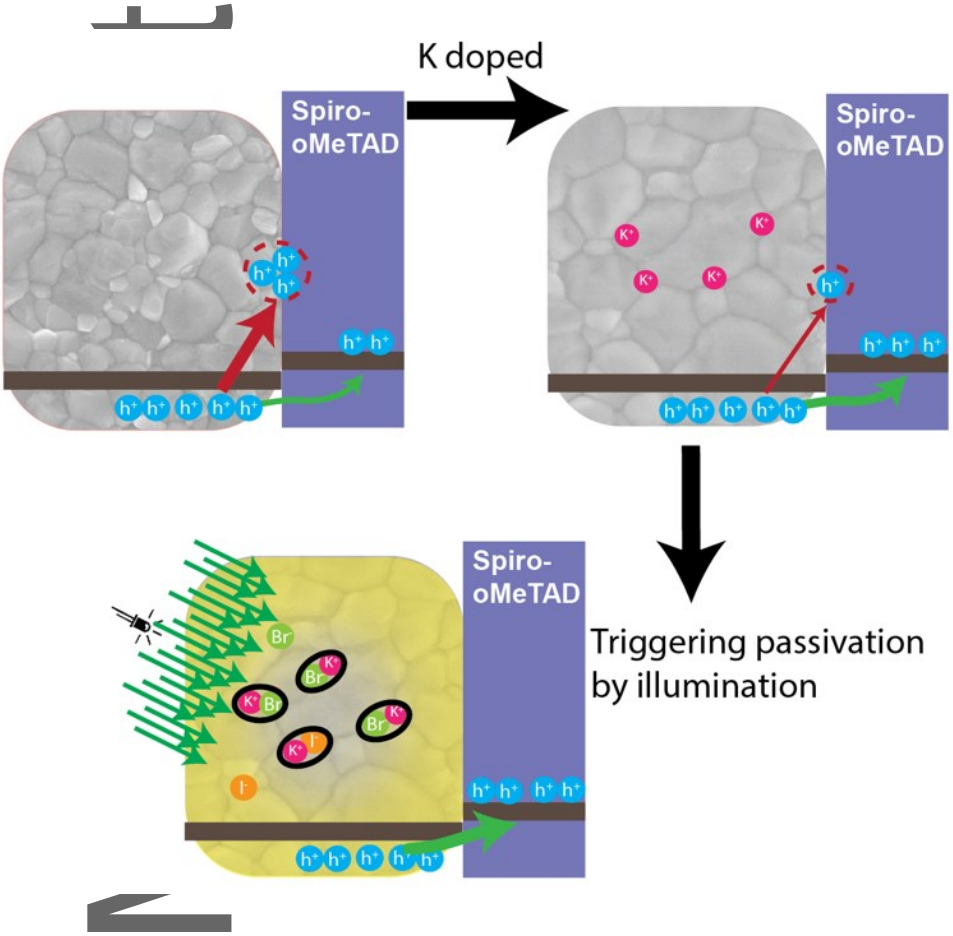

The passivation effect of K^+ doping in mixed-cation mixed-halide perovskite is triggered by light illumination to form stable KBr-like compounds and reduce the interface trapping defect density to facilitate a high efficiency and hysteresis-free perovskite solar cell.